Insight into the structure and localization of the titania overlayer in TiO_2-coated SBA-15 materials

Fuxiang Zhang,[ab] Xavier Carrier,[ab] Jean-Marc Krafft,[ab] Yuji Yoshimura[c] and Juliette Blanchard*[ab]

Received (in Montpellier, France) 31st August 2009, Accepted 17th November 2009
First published as an Advance Article on the web 18th January 2010
DOI: 10.1039/b9nj00439d

Titania-coated SBA-15 materials (Ti-SBA-*n* with $n = 1$–4) were synthesized by successive grafting of titanium isopropoxide in iso-propanol. The investigation of the nature and localization of the TiO_2 overlayer allowed us to conclude that there was formation of very small (UV-visible, EXAFS, XANES), *ca.* 2 nm or smaller (XRD and TEM) TiO_2 domains that cover only partially the silica surface (CO adsorption). These nano TiO_2 domains are located on or close to the mesopore surface (EELS, XRD and N_2-sorption) rather than in the micropores as previously reported.

1. Introduction

TiO_2 is widely used in the field of catalysis as photocatalyst, conventional catalyst (Claus reaction) and catalyst support for metal, metal oxide or metal sulfide for a wide range of applications (reduction of NO_x,[1,2] oxidation,[3] hydrodesulfurization,[4,5]...). For all these applications, high surface area is desired and TiO_2 nanoparticles are often employed. However their application is hindered by the low thermal stability of the nanoparticles and, for applications in solution, by their tendency to agglomerate and their difficult recovery. To overcome this difficulty TiO_2 can be anchored on high surface area oxides with good thermal stability. Among potential supports, silica is often chosen, and more specifically ordered SBA-15 mesoporous silica materials, to take advantage of their high surface area (up to 800 $m^2\ g^{-1}$) and large pores size (4–10 nm).[6–13] The most common methods used for the incorporation of titania in mesoporous silica are:

– Direct synthesis (*i.e.* addition of the titania precursor to the silica source during the synthesis of the mesoporous material). This procedure is generally used when the incorporation of a small amount of isolated Ti in the SBA-15 walls is desired.[6]

– Impregnation using either incipient wetness method followed by drying (which generally leads to a poor dispersion of the deposited phase),[7] or more elaborate procedures such as impregnation with a colloidal TiO_2 suspension[8] or impregnation followed by controlled hydrolysis[9] (both methods result in the deposition of TiO_2 particles with controlled size in the range 3–7 nm). However, impregnation generally leads to a partial blocking of the pores of the SBA-15 materials.

– Grafting is also sometimes described as surface sol–gel synthesis.[10,11] It involves the reaction between a surface silanol and a titanium alkoxide (similar to the condensation reaction in sol–gel chemistry). This procedure can be repeated several times to increase the loading.[11–13] A "clean" grafting necessitates the removal of any trace of water (to prevent the formation of unsupported TiO_2 particles by hydrolysis of $Ti(OR)_4$). Compared to impregnation, grafting generally leads to a better dispersion of the deposited TiO_2 and avoids pore blocking of the SBA-15 support by the deposited phase.

Nevertheless, the exact nature and localization of the TiO_2 phase on the SBA-15 support remain unclear. Earlier reports concluded that there was grafting of isolated species at low loading followed by the formation of a homogeneous coating at higher loading.[10,14,15] However, recent studies suggested that grafting rather results in the formation of very small (<2 nm) TiO_2 domains and assigned the stabilization of these nanodomains to the micropores of SBA-15. SBA-15 materials indeed present a double porosity: 2D ordered mesopores (pore diameter 4–8 nm) and a microporous corona made of disordered pores, a fraction of which connect the mesopores.[16] According to Zukerman *et al.*,[17] who compared two TiO_2/SBA-15 samples prepared using SBA-15 materials with different microporosity, the presence of micropores decreases the crystallization temperature of anatase and improves the dispersion of TiO_2. According to Wang *et al.*[7] and Perathoner *et al.*,[18] for TiO_2 loadings lower than 15 wt%, grafting occurs exclusively in the microporous corona, leading, after calcination, to the formation of TiO_2-like (probably Si doped) nanoareas (1–2 nm).

In the present study, titania-coated SBA-15 materials were prepared by successive grafting of titanium alkoxide (1 to 4 graftings). These samples were compared with a TiO_2/SBA-15 sample prepared by incipient wetness impregnation. In order to get a deeper insight into the nature and localization of the TiO_2 overlayer, TiO_2-coated and TiO_2-impregnated materials were examined using XRD, N_2-adsorption, UV-visible spectroscopy, TEM, EDX, EXAFS, XANES and low temperature CO adsorption followed by FTIR.

[a] *UPMC Université Paris 06, UMR 7197, Laboratoire de Réactivité de Surface, F-75005 Paris, France*
[b] *CNRS UMR 7197, Laboratoire de Réactivité de Surface, F-75005 Paris, France. E-mail: juliette.blanchard@upmc.fr; Fax: +33 144276033; Tel: +33 144273630*
[c] *Hydrotreating Catalysis, Research Center for New Fuels and Vehicle Technology, National Institute of Advanced Industrial Science and Technology, Ibaraki 305-8565, Japan*

Experimental

Sample preparation

SBA-15 mesoporous silica. The SBA-15 mesoporous silica was prepared following the method reported by Zhao *et al.*[19] as described in ref. 20. The hexagonal P6mm symmetry of the mesoporous material was confirmed with XRD. N_2-sorption yields a specific surface area of 789 $m^2\ g^{-1}$, a narrow pore size distribution (FWHM = 15 Å) and an average pore size of 62 Å (BJH analysis on the desorption branch of the isotherm).

Ti grafting. For each grafting, $Ti(O^iPr)_4$ (Aldrich) was dissolved in anhydrous isopropanol (Fluka). The amount of dissolved $Ti(OPr^i)_4$ was adjusted to a surface density of 10 μmol m^{-2} corresponding to a large stoichiometry excess with regards to the density of surface silanols (3–4 μmol m^{-2}). The SBA-15 support was previously dehydrated at high temperature (450 °C, 4 h) to ensure the complete removal of both physisorbed and hydrogen-bonded water not only from the mesopores but also from the micropores of the SBA-15 materials.[21] The dehydrated SBA-15 was added to the $Ti(OPr^i)_4$ solution and the suspension was stirred overnight under argon, filtrated and washed with equal volume of dry isopropanol. The solid was then dried at 100 °C and calcined at 500 °C for 6 h. The whole procedure was repeated three more times to increase the titania loading. The samples are designated as Ti-SBA-*n*, where *n* stands for the number of graftings (*n* = 1–4). A sample was prepared by incipient wetness impregnation with the same TiO_2 loading as the sample Ti-SBA-4. This sample is designated as Ti-SBA-IWI. TiO_2 loadings for all samples are reported in Table 1. TiO_2 P25 from Degussa (anatase ≈ 80%, rutile ≈ 20%, S_{BET} ≈ 50 $m^2\ g^{-1}$, particle diameter ≈ 25 nm)[22] was used as TiO_2 reference. To examine their thermal stability Ti-SBA-4 and Ti-SBA-IWI were further calcined at 700 and 900 °C (heating rate of 1 °C min^{-1}); the obtained samples are denoted as Ti-SBA-4 (*T*) and Ti-SBA-IWI (*T*), respectively (where *T* stands for the calcination temperature).

Characterization

XRD measurements were carried out using a D8 Advance Powder diffractometer with Cu-Kα radiation (λ = 1.54 Å). The scanning range was 0.5–3° (2θ) for small angle, and 10–90° (2θ) for wide angle measurements with a step size of 0.01° (small angle domain) and 0.02° (wide angle domain).

N_2 adsorption–desorption isotherms were collected on an ASAP 2010 analyzer (Micromeritics). Prior to analysis, the samples were degassed ($p < 1$ Pa) at 150 °C (for SBA-15) or 220 °C (for titania-grafted materials) for 5 h. The microporous volume (V_{micro}) and the mesoporous surface area (S_{meso}) were estimated from a *t*-plot (Harkin–Jura) analysis of the adsorption curve (0.35 nm < *t* < 0.65 nm, *t* being the statistical thickness). The "microporous" surface area (S_{micro}) was calculated as $A_{micro} = A_{BET} - A_{meso}$. The pore size distribution was calculated from the desorption branch of the isotherm using the BJH model.

UV-Vis spectra were recorded in the 190–700 nm range on a Cary 5 spectrometer equipped with an integration sphere. Before measurement, the samples were dehydrated at 500 °C for 4 h. UV-vis measurements were performed in the diffuse reflectance mode (*R*) and transformed to a magnitude proportional to the extinction coefficient through the Kubelka–Munk function *F*(*R*). Band-gap values (E_g) were obtained by fitting the linear domain of the plot $(F(R)E)^n$ *versus* the energy of the absorbed light *E*. The value of *n* was set to 0.5 assuming an indirect transition between the top of the valence band and the bottom of the conduction band.[23,24] Other authors have proposed, for TiO_2/SiO_2 mixed oxides, to consider TiO_2 as a direct semi-conductor (*i.e.* to use a value of 2 for *n*). However, using this value the linearity was less pronounced and the obtained E_g value of bulk TiO_2 (P25) (E_g = 3.60 eV) was far from the value of bulk anatase (E_g = 3.23 eV).

TEM, Selected Area Electron Diffraction (SAED) and Energy Dispersive X-ray Spectroscopy (EDS) of microtomed samples were obtained on a JEOL JEM 2011 apparatus with an accelerating voltage of 200 kV. Elemental mapping using energy filtered TEM (EELS) was performed using a JEOL 2100 FEG equipped with a Gatan imaging filter (GIF 2001).

Ti K-edge (4.965 KeV) X-ray absorption spectra were measured at Photon Factory (Institute for Material Structure Science, High Energy Accelerator Organization, KEK-IMSS-PF, Japan) on beamline BL-9. The samples were freshly calcined before the experiment. Wafers (10 mm diameter) were prepared by diluting the sample in an inert matrix: 3 mg of TiO_2 or 6 mg of Ti-SBA-1 (or Ti-SBA-4) were diluted in 35 mg cellulose, in order to get an edge jump Δμ(*E*) close to 1.

Table 1 Textural parameters of the Ti-SBA-*n* and Ti-SBA-IWI materials

Sample	TiO_2[a] (wt%)	S_{BET}[b] ($m^2\ g^{-1}$)	S_{micro}[c] ($m^2\ g^{-1}$)	S_{meso}[c] ($m^2\ g^{-1}$)	V_{micro}[b] ($cm^3\ g^{-1}$)	D[d] (Å)	V_{meso}[e] ($cm^3\ g^{-1}$)
SBA-15	—	789	193	596	0.075	62	0.9
Ti-SBA-1	12 (11 ± 0.5)	614 (697)	144 (−25%)	470 (−21%)	0.057	58	0.71
Ti-SBA-2	24	548 (721)	121 (−37%)	426 (−29%)	0.048	53	0.63
Ti-SBA-3	30	453 (647)	93 (−52%)	359 (−40%)	0.037	48	0.51
Ti-SBA-4	34 (33 ± 0.6)	392 (593)	74 (−62%)	312 (−48%)	0.029	42	0.42
Ti-SBA-IWI	35	450 (692)	80 (60%)	370 (−38%)	0.031	39	0.45

[a] TiO_2 loading was measured by ICP and confirmed by EDX for Ti-SBA-1 and Ti-SBA-4 by EDS (values in brackets). [b] The value in brackets is corrected from the contribution of TiO_2 in the weight of the grafted material ($X_{corrected} = X/(1 - wt\%TiO_2)$) as proposed by Landau *et al.*[9] [c] See Experimental for details; the values in brackets are the relative decrease (%) in surface area compared to the starting SBA-15. [d] The mesopore diameter is taken at the maximum of the pore size distribution calculated using the BJH model on the desorption curve. [e] $V_{meso} = V_{tot} - V_{micro}$ (V_{tot} being the volume adsorbed at $P/P^0 = 0.97$).

Extended X-ray absorption fine structure (EXAFS) oscillations were extracted from the raw data using Athena software[25,26] by background subtraction (Autobk algorithm) and normalization with the edge height. E_0 was chosen at the maximum of the $\mu(E)$ first derivative. Fourier transforms to R space of the k^3-weighted EXAFS data were done in the k range of 1–12 Å using the Hanning window function (dk = 0.5 Å^{-1}), where "k" indicates a photoelectron wave number and "R" represents the distance between the absorber atom and a neighbor scatterer atom. EXAFS data were analyzed using Artemis software[25,26] over the k range of 2–12 Å^{-1} and R range of 1–3 Å. The maximum number of independent points can be estimated from the expression $IP = [(2\,\Delta k\,\Delta R/\pi) + 1]$, where Δk is the extent of the data in k-space and ΔR the R range to be modeled. The number of variables used for the analysis (8) remained well below the number of independent points (IP = 12). The values of $F_j(k)$, $\delta_j(k)$ and $\lambda_j(k)$ for Ti–O and Ti–Ti pairs were generated by the Atoms 2.5[27] and FEFF 8.0[28] codes using the crystallographic data of TiO_2 anatase. Fitting was performed in R-space. During the fitting procedure of the Ti-SBA-n samples the coordination number (N), bond distance (R) and Debye–Waller factor (σ^2) were allowed to vary freely. The amplitude reduction factor (S_0^2) was determined experimentally on the reference TiO_2 sample and held constant afterwards at $S_0^2 = 0.84$.

Transmission FTIR spectra of adsorbed CO were collected on a Bruker Vector 22 spectrometer using a MCT detector (resolution 2 cm^{-1}, 32 scans per spectrum). Self-supported wafers of about 15 mg cm^{-2} were first calcined *in situ* under N_2 (100 mL min^{-1}) at 723 K and then evacuated (10^{-2}–10^{-3} mbar) at 723 K for 1 h. The IR cell was then cooled down to *ca.* 100 K. Prior to addition of CO pulses, an He pulse (0.3 μmol) was added to help establish the temperature equilibrium.[29] The contribution of water was subtracted from each spectrum and the coefficient of this subtraction was adjusted in order to minimize the rotation bands of water. All the CO spectra presented herein correspond to difference spectra, *i.e.* spectrum after CO adsorption minus spectrum after addition of the He pulse.

Results

Structure of TiO_2/SBA-15

Fig. 1 shows the XRD patterns of SBA-15, Ti-SBA-n ($1 \leq n \leq 4$) and Ti-SBA-IWI materials at low angles. The three characteristic (100), (110) and (200) reflections of the SBA-15 materials are observed on all grafted samples, indicating that the mesostructure of SBA-15 is well preserved after titania graftings. The position of the (100) reflection is almost unchanged after grafting: $\theta = 0.91°$ (d = 97 Å) for SBA-15 and $\theta = 0.93°$ (d = 95 Å) for the Ti-grafted samples. Graftings lead to a moderate decrease in the intensities of all reflections. However, this phenomenon could simply be due to X-ray absorption by the TiO_2 phase. The main evolution with the number of graftings is the decrease in the ratio of the intensities of the (110) and (200) peaks. Changes in the relative intensities of these two peaks are commonly observed on SBA-15 materials. For example Kruk *et al.*[30] observed that,

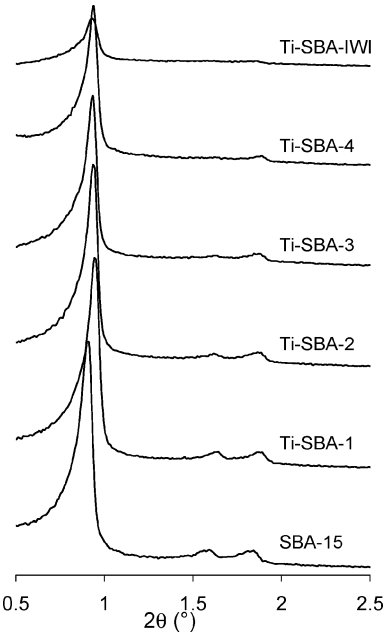

Fig. 1 Small-angle XRD patterns of titania-impregnated sample (Ti-SBA-IWI), titania-grafted samples (Ti-SBA-n, $1 \leq n \leq 4$) and parent SBA-15.

during SBA-15 synthesis, the intensity of the (110) reflection is very low compared to that of the (200) reflection if the synthesis is conducted at low temperature, whereas the (110) reflection is more intense than the (200) reflection for syntheses conducted at high temperature. They assigned these variations to a change in the thickness of the silica walls (the thicker the wall, the more intense the (200) reflection). The decrease in the (110) relative intensity with the number of graftings could therefore be associated with the deposition of TiO_2 on the surface of the SBA-15 pores, leading to a thickening of the walls. The pattern of the impregnated sample (Ti-SBA-IWI) shows a pronounced decrease in the intensities of all reflections although this sample contains the same TiO_2 loading as Ti-SBA-4. As proposed by Schüth *et al.*,[31] this loss of intensity is probably due to a loss of contrast between walls and pores induced by the filling of the SBA-15 pores with TiO_2.

Whatever the number of graftings, the anatase reflections are absent from the wide angle XRD patterns of the grafted samples (see the pattern of Ti-SBA-4 on Fig. 2 as an example), whereas sharp reflections, characteristic of large anatase particles, are clearly observed on the pattern of Ti-SBA-IWI. The size threshold for the observation of nanoparticles using XRD is usually considered to be *ca.* 3 nm. However, in the case of anatase nanoparticles, XRD peaks were observed by Monticone *et al.*[32] for particles with diameter as small as 1.5 nm. The absence of diffraction peaks on the XRD patterns of the Ti-SBA-n materials indicates therefore the formation either of very small anatase particles or of amorphous particles. As already stated by Perathoner *et al.*,[18] the absence of XRD detectable particles after calcination at 500 °C is already a clear indication of the stabilizing role of the silicic support. The anatase reflections are detected on grafted samples only after calcination to high temperature (900 °C) and the size of the crystallites (evaluated using the Debye

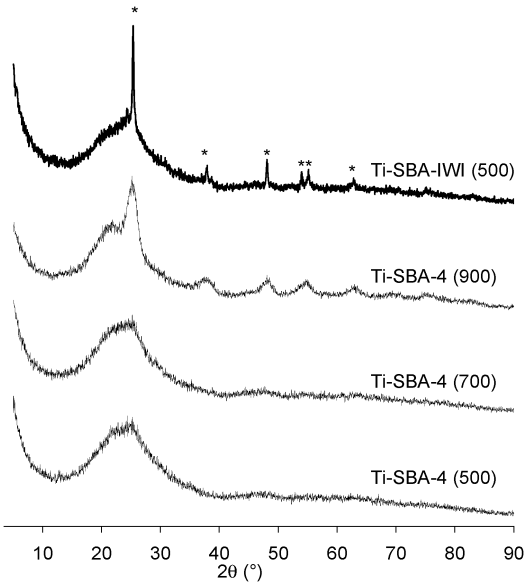

Fig. 2 Wide-angle XRD patterns of Ti-SBA-4 and Ti-SBA-IWI samples (the value in brackets is the calcination temperature). The * mark the anatase reflections.

Sherrer formula on the (101) reflection), remains small (*ca.* 4–5 nm). Whatever the preparation procedure (impregnation or grafting), no transition to rutile occurs, even after calcination at 900 °C.

Nature and localization of the TiO_2 coating

Fig. 3 shows the diffuse reflectance UV-Vis spectra of the grafted samples together with those of the reference TiO_2 and Ti-SBA-IWI. The maximum of the absorption spectra and the corresponding band edge (see Experimental for details about the determination of the edge) are summarized in Table 2. The band maximum of the grafted and impregnated samples is blue shifted compared to bulk TiO_2 in the order Ti-SBA-1 > Ti-SBA-2 ≈ Ti-SBA-3 ≈ Ti-SBA-4 > Ti-SBA-IWI > TiO_2.

UV-Visible spectroscopy is commonly used to investigate the size of the TiO_2 particles since for pure anatase or rutile particles the bandgap energy (E_g) is expected to shift with the particle size according to the relationship:

$$\Delta E_g = (4h^2\pi^2/2\mu d^2) - (3.6e^2/\varepsilon d)$$

where h is the Planck constant, e the elementary charge, ε the dielectric constant of TiO_2, d the TiO_2 particle diameter and μ is defined as $\mu^{-1} = m_e^{-1} + m_h^{-1}$ where m_e and m_h are the anatase TiO_2 electron and hole effective masses.

Wang *et al.*[12] proposed to use this equation for the determination of the size of TiO_2 nanoparticles supported on SBA-15 and found, using the following set of parameters: $m_e = 8m_0$, $m_h = 3m_0$ (where m_0 is the free electron mass) and $\varepsilon \approx 150$, a particle size of 1.3 nm after three successive graftings. The TiO_2 particle size calculated for the Ti-SBA-*n* samples using the same set of parameters varies between 1.4 nm (Ti-SBA-1) and 1.6 nm (Ti-SBA-2, Ti-SBA-3 and Ti-SBA-4). However, Lassaletta *et al.*[33] and Gao *et al.*[34] pointed out that this type of calculation could underestimate the size of TiO_2 particles in titania–silica mixed oxide. Indeed,

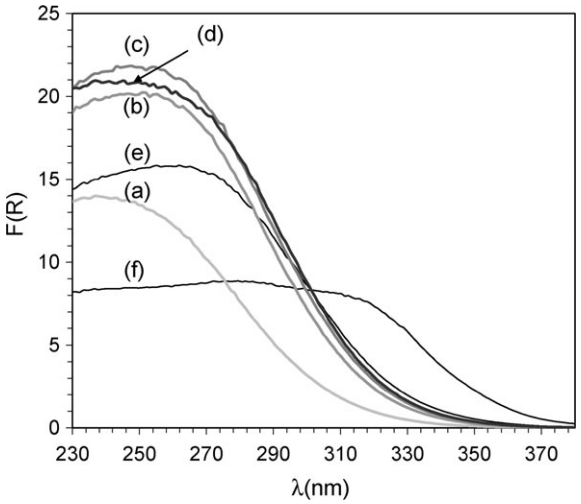

Fig. 3 UV-Vis spectra of (a) Ti-SBA-1; (b) Ti-SBA-2; (c) TiSBA-3, (d) Ti-SBA-4, (e) Ti-SBA-IWI, (f) TiO_2.

Table 2 Band maximum and edge energy of grafted samples

Sample	E_g/eV[a]	Band max/nm
TiO_2 (P25)	3.20	306
Ti-SBA-1	3.63	237
Ti-SBA-2	3.55	250
Ti-SBA-3	3.52	250
Ti-SBA-4	3.52	250
Ti-SBA-IWI	3.46	258

[a] The method used for the determination of E_g is described in the Experimental.

for supported TiO_2 particles, the position of the bandgap is, according to these authors, the result of a combination of the quantum size effect and of an effect of the chemical environment of Ti. Thus, according to Gao *et al.*[35] who studied TiO_2 particles supported on fumed silica, the band shift with the Ti loading is due to an increase in Ti coordination for low to intermediate Ti loading, whereas it is due to an increase in the number of Ti nearest neighbors for intermediate to high TiO_2 loading. As a consequence, in our case, the shift in the bandgap energy with the number of graftings reflects to some extent an increase in the size of the TiO_2 domains but cannot be used to determine it quantitatively.

Typical bright field TEM images of Ti-SBA-1 and Ti-SBA-4 are shown in Fig. 4. These images are further evidences for the preservation of the mesostructure and show no large titania particles on the outer surface of SBA-15, in agreement with the absence of anatase XRD reflections. Very small (*ca.* 2–3 nm) crystalline TiO_2 particles can be detected at high magnification (Fig. 4c) but they may not be representative of the whole sample. Indeed in spite of the high TiO_2 loading of Ti-SBA-4, very few crystalline particles are observed. On the Ti-SBA-IWI sample (Fig. 4d), the morphology of deposited titania is very different with a large amount of particles on the outer surface of the SBA-15 support. These particles were identified as anatase using microdiffraction (Fig. 4d, inset).

The TiO_2 content in Ti-SBA-1 and Ti-SBA-4 was analyzed on three different areas by EDS. TiO_2 was found to be

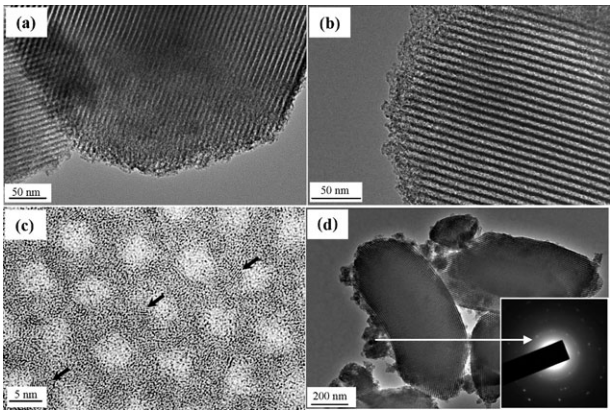

Fig. 4 Representative TEM images of several samples: (a) Ti-SBA-1; (b) and (c) Ti-SBA-4 (arrows show crystalline TiO_2 nanoparticles); (d) Ti-SBA-IWI (inset: microdiffraction pattern on one of the particles observed outside the SBA-15 grains).

homogeneously distributed on the support with a loading close to that obtained by ICP analysis (Table 1). This indicates a homogeneous distribution of the deposited titania on the surface of SBA-15.

Energy-filtered TEM (EELS) at high magnification was used to gain a deeper insight into the localization of titania, *via* the high resolution mapping of Ti and Si elements (see Fig. 5b for Si mapping and 5c for Ti mapping). The overlap of the Si and Ti elemental maps (Fig. 5d) clearly shows that titania is homogeneously distributed in the Si poor areas of the SBA-15 materials, *i.e.* close to or on the surface of the mesopores.

The even coating of titania in the channel of SBA-15 can be further demonstrated by the comparison of N_2 sorption isotherms of SBA-15 and Ti-SBA-*n* ($1 \leq n \leq 4$) samples. SBA-15 shows typical type IV adsorption isotherms (Fig. 6a)

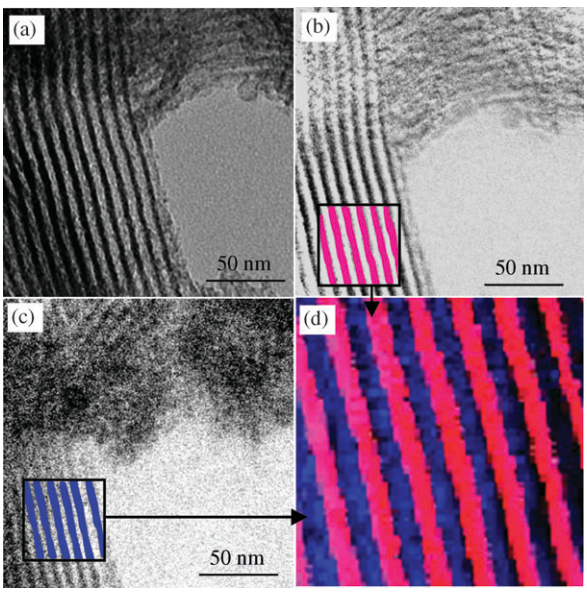

Fig. 5 EELS (Energy-Filtered TEM) images of a zone of Ti-SBA-4 using (a) zero loss filtration; (b) Si elemental mapping; (c) Ti elemental mapping; (d) overlap of Si and Ti elemental maps.

with a well-defined step around $P/P_0 = 0.7$, characteristic of capillary condensation within uniform pores. The shape of the isotherm is retained for Ti-SBA-*n* samples but the onset of the capillary condensation is progressively shifted toward lower P/P_0 values upon increasing the number of graftings. This result is confirmed by the BJH analysis of the desorption curve (Fig. 6b) which shows a progressive decrease in the maximum of the pore size distribution but no significant modification of its full width at half maximum. By contrast, the shape of the N_2 sorption curve of Ti-SBA-IWI is distorted, and its pore size distribution complex (the pore size distribution maximum at 39.2 Å is an artifact associated with the instability of the nitrogen meniscus below $P/P_0 = 0.42$). This indicates that the uniform structure of the mesopores has not been preserved and could reflect the formation of large TiO_2 particles inside the SBA-15 pores.

The mesoporous and microporous surface areas and the pore diameter decrease regularly with the number of graftings Fig. 7 and Table 1). It is worth mentioning that after the 4th grafting, the Ti-SBA-4 material still retains a BET surface area of *ca.* 392 $m^2\ g^{-1}$ and pore diameter of *ca.* 42 Å. This reduction in the mesopore diameter could reflect the presence of a titania layer inside the SBA-15 mesopores. Indeed, the increase in the pore walls thickness ($e = \frac{2d}{\sqrt{3}} - D$ with d the d-spacing and D the pore diameter) from 50 Å for the SBA-15 to 67 Å for the Ti-SBA-4, is consistent with the formation of one TiO_2 monolayer (10.5 Å).

To gain further insight into the local environment of the titanium atoms, XANES and EXAFS spectra at the Ti K-edge of dehydrated TiO_2, Ti-SBA-1 and Ti-SBA-4 were examined. The pre-edge spectra (Fig. 8a) of the TiO_2 reference material is characteristic of octahedral Ti with the presence of 3 weak maxima at 4965.7, 4968.7 and 4971.1 eV that have been assigned to transitions from the 1s core level of Ti to t_{2g}, e_g and a_{1g} levels, respectively.[36,37] XANES spectra of the grafted samples differ significantly from that of reference TiO_2 with one main peak at 4667.7 eV and a shoulder at 4971.1 eV. According to Farges *et al.*,[37] the position and the intensity of the main peak reflects the coordination of Ti. As reported by Gao *et al.*,[35] the pre-edge feature of supported titania is most probably a mixture of at least two Ti coordinations. However, the position and intensity of the pre-edge features of Ti-SBA-1 and Ti-SBA-4 allow us to exclude the presence of 4-fold coordinated Ti (except as very minority species) and to conclude the presence of octahedral and pentacoordinated Ti on the grafted samples. As the pre-edge of Ti-SBA-1 and Ti-SBA-4 are very similar, one can propose that the nature of the TiO_2 overlayer does not differ significantly in both samples. EXAFS spectra at the Ti K-edge of TiO_2, Ti-SBA-1 and Ti-SBA-4 are shown on Fig. 8b. Three types of neighbors can be observed on the spectrum of TiO_2: the peak at short distance corresponds to the 6 O neighbors at 1.94–1.97 Å, the peak at intermediate distance is assigned to the 4 Ti neighbors at 3.05 Å and the peak at long distance to the 4 Ti neighbors at 3.78 Å. Comparatively, the spectra of the grafted samples show a lower intensity for the peak assigned to the O shell and a decrease to almost zero for the peaks corresponding to the Ti shells. The fitted parameters for the O shell and the first Ti shell are reported in Table 3. Due to the large uncertainty on

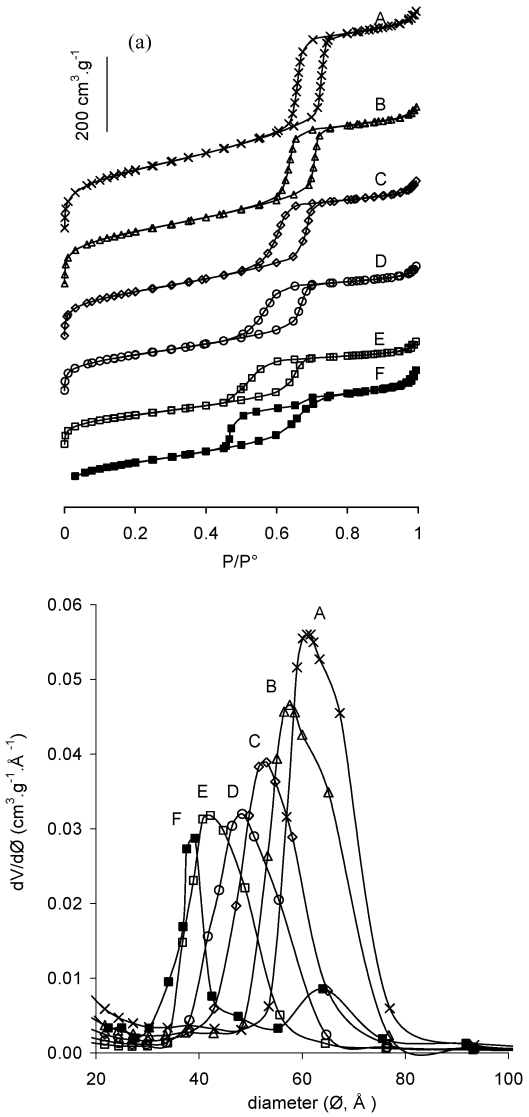

Fig. 6 (a) Nitrogen adsorption–desorption isotherms and (b) pore size distribution (BJH calculation on the desorption curve) of A: SBA-15, B–E: Ti-grafted SBA-15 (Ti-SBA-1 to Ti-SBA-4) and F: Ti-SBA-IWI.

the N values, it is difficult to establish precisely the coordination of Ti from the number of O neighbors in the first shell. However, according to Gao *et al.*,[34] it is possible to use the Ti–O bond length (1.88 Å for Ti-SBA-1 and 1.92 Å for Ti-SBA-4) as a signature of the coordination of Ti: a bond length of 1.80–1.84 Å is characteristic of fourfold coordinated Ti, a bond length of 1.89–1.91 Å characteristic of fivefold coordinated Ti and a bond length of 1.95–1.96 Å of 6-fold coordinated Ti. We can therefore conclude that the 5-fold coordination is predominant for our samples. This indicates that, even after the 1st grafting, Ti atoms are mostly located in TiO_2 domains, with very few—if any—Ti atoms inserted in tetrahedral coordination in the silica walls. A slight increase in the Ti coordination (and as a consequence of the size of the TiO_2 domains) between the 1st and 4th grafting is likely considering the increase in the Ti–O bond length and the increase in the number of O and Ti neighbors.

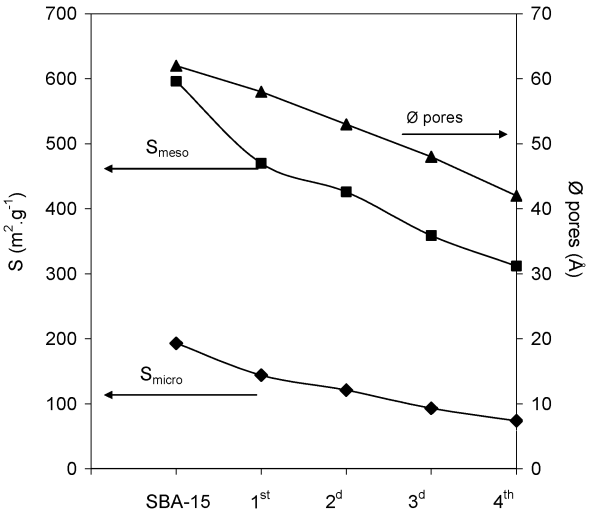

Fig. 7 Evolution of the mesoporous surface area (S_{meso}), the microporous surface area (S_{micro}) and of the pore diameter (Ø pores) with the number of graftings.

FTIR of adsorbed CO was used to investigate the surface sites of Ti-SBA-4. CO is indeed a weak base that interacts with Brønsted and Lewis sites at low temperature (*ca.* 100 K) and the position of the ν(CO) band shifts with the strength of the acid sites.[38] Fig. 9 shows the difference spectra in the ν(CO) range of SBA-15, Ti-SBA-4 and TiO_2 (P25 Degussa, anatase 80%) after addition of 25, 200 and 550 μmol g^{-1} of CO. On the spectra obtained for SBA-15 (Fig. 9a), two bands are observed whatever the amount of CO that can be assigned to CO adsorbed on silanol (ν(CO) = 2157 cm^{-1}, associated in the ν(OH) range with a positive band at 3658 cm^{-1}) and to physisorbed CO (ν(CO) = 2137 cm^{-1}). For TiO_2 (Fig. 9c), two bands are observed at 2211 and 2193 cm^{-1} after addition of 25 μmol g^{-1} CO. After addition of 200 μmol g^{-1} CO these bands shift to 2208 and 2181 cm^{-1}. After addition of 550 μmol g^{-1} CO, they shift further to 2207 and 2180 cm^{-1} and a third band is observed at 2167 cm^{-1}. These bands can be unambiguously attributed to CO adsorbed on Lewis sites since the ν(OH) range of the spectra is not modified. Hadjiivanov and coworkers,[39] have proposed the following assignments for these bands: the band that shifts from 2211 cm^{-1} to 2208 cm^{-1} corresponds to CO adsorbed on 4-coordinated Ti^{4+} (α sites, strong Lewis sites); the one that shifts from 2193 to 2180 cm^{-1} is associated with CO bonded to 5-coordinated Ti^{4+} on (100) and (101) surfaces (β′ and β′′ sites, mild Lewis sites); the band at 2167 cm^{-1} is attributed to CO on 5-coordinated Ti^{4+} on (001) surfaces and on some edges (γ sites, weak Lewis sites). The IR spectrum of Ti-SBA-4 shows two bands after addition of 25 μmol g^{-1} CO at 2192 and 2165 cm^{-1}. They shift to 2187 and 2163 cm^{-1} after addition of 200 μmol g^{-1} CO. In the ν(OH) range (Fig. 9d) the spectrum shows a main band at 3652 cm^{-1} with a shoulder at 3590–3600 cm^{-1}. After addition of 550 μmol g^{-1} CO, a new band is observed at 2137 cm^{-1}, which can be assigned to physisorbed CO, whereas the existing bands shift to 2183 cm^{-1} and 2160 cm^{-1}. In the ν(OH) range (not shown) an intense band at 3650 cm^{-1} is observed. The band shifting from 2192 to 2183 cm^{-1} can be assigned, by analogy with the work of Hadjiivanov and coworkers,[39] to CO

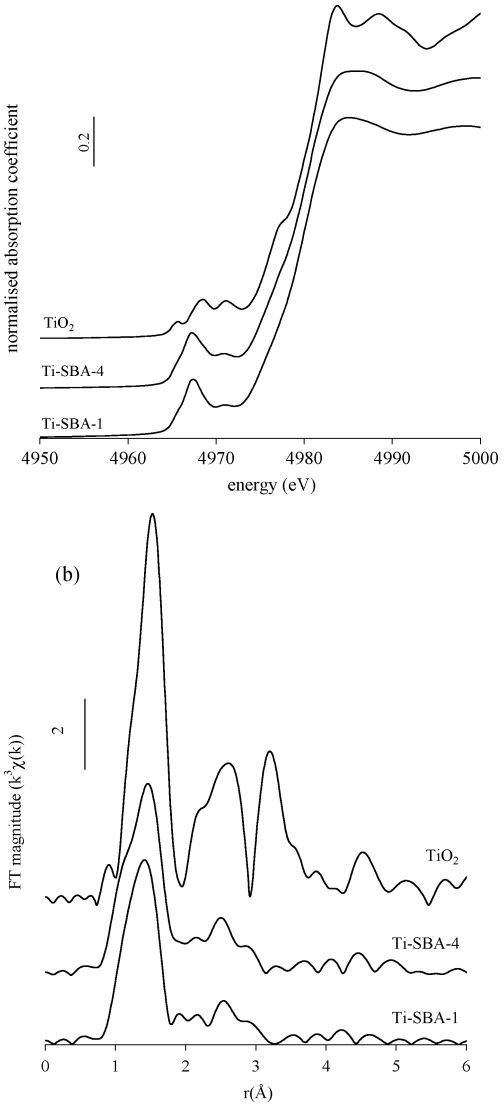

Fig. 8 (a) XANES and (b) EXAFS spectra at the Ti K-edge of TiO_2, Ti-SBA-1 and Ti-SBA-4.

on β′ and β″ sites of anatase like domains. In the ν(OH) range, the positive band at 3652 cm^{-1} observed after addition of 200 μmol g^{-1} CO indicates the presence of silanol groups similar to those of pure silica. A band at 2157 cm^{-1} is therefore expected in the ν(CO) range. The fitting of this spectrum (Fig. 9b) confirms the presence of this band together with another band at 2165 cm^{-1}. The envelope of these two bands is the band observed at 2163 cm^{-1}. This composite band shifts from 2163 to 2160 cm^{-1} after introduction of 550 μmol g^{-1} CO due the growth of the component associated with CO adsorbed on silanols. Two suggestions can be made regarding the assignment of the band at 2165 cm^{-1}. First it can be assigned to weak Lewis sites of the TiO_2 supported phase similar to the γ sites of anatase (the ν(CO) band associated with these sites was reported at 2165 cm^{-1} in ref. 39 and observed at 2167 cm^{-1} in this work). Compared to the spectra of TiO_2, the relative intensity of the 2165 cm^{-1} band is significantly higher and the band at 2211–2208 cm^{-1} assigned to the strong Lewis sites in bulk TiO_2 is missing. This could indicate that the morphology of the supported TiO_2 particles is different from that of unsupported TiO_2 nanoparticles. Alternatively, the band at 2165 cm^{-1} can be assigned to CO adsorbed on weak Brønsted sites and associated in the ν(OH) range with the shoulder at 3590–3600 cm^{-1}. These weak Brønsted sites are either Ti–OH, as proposed in ref. 29 for TiO_2–SiO_2 mixed oxides, or Si–OH groups having titanium atoms in their close vicinity, as suggested in ref. 40 for TiO_2 supported on SiO_2. As these weak Brønsted sites have not been observed on pure TiO_2 (either anatase or rutile) their presence would indicate that, besides the silica-like domains (whose presence is evidenced by the two bands at 3652 cm^{-1} and 2157 cm^{-1}) and titania-like domains (whose presence is demonstrated by the band at 2192–2183 cm^{-1}), mixed oxide domains are also present on Ti-SBA-4.

Discussion

Grafting step

It is interesting to compare the amount of grafted TiO_2 after the first grafting with the amount of Si–OH in a SBA-15 material. There are relatively few reports on a quantitative determination of the silanol density in SBA-15 materials. In ref. 41, Shi *et al.* determined the amount of silanols in a dehydrated SBA-15 sample (150 °C, 2 h)[42] using ^{1}H MAS NMR. They calculated the following composition: $SiO_{1.92}(OH)_{0.16}$, which corresponds to a surface density of silanols of 2.15 SiOH per nm^2 (taking into account the surface area of the SBA-15 material used for the experiment: 706 m^2 g^{-1}).[42] This value is close but slightly lower than the values reported by Mueller *et al.*[43] for non porous silica using thermogravimetric analysis (2.5 to 3.5 OH per nm^2). 2.15 SiOH per nm^2 corresponds to a concentration of silanols of 2.85 mmol g^{-1} in the SBA-15 used in the present study (789 m^2 g^{-1}). However, considering the temperature of the pretreatment before grafting (450 °C) we can expect a partial

Table 3 Fitted structural parameters from EXAFS spectra of Ti-SBA-1, Ti-SBA-4 and reference TiO_2

	Scatterer	N	R (pm)	ΔE_0 (eV)	$\sigma^2/10^{-4}$ Å^2	$\mathscr{R}$-factor
TiO_2	O	6	197(1)	2(1)	67(9)	2%
($S_0^2 = 0.84$)	Ti	4	300(1)	−7(2)	86(10)	
Ti-SBA-1	O	4.4(0.8)	188(1)	−5(3)	110(21)	2%
	Ti	0.7(0.6)	304(5)	−8(8)	54(58)	
Ti-SBA-4	O	5.0(0.9)	192(2)	−1(2)	124(23)	2.5%
	Ti	2.8(1)	302(2)	−9(8)	77(45)	

The values in brackets are the uncertainties of calculation.

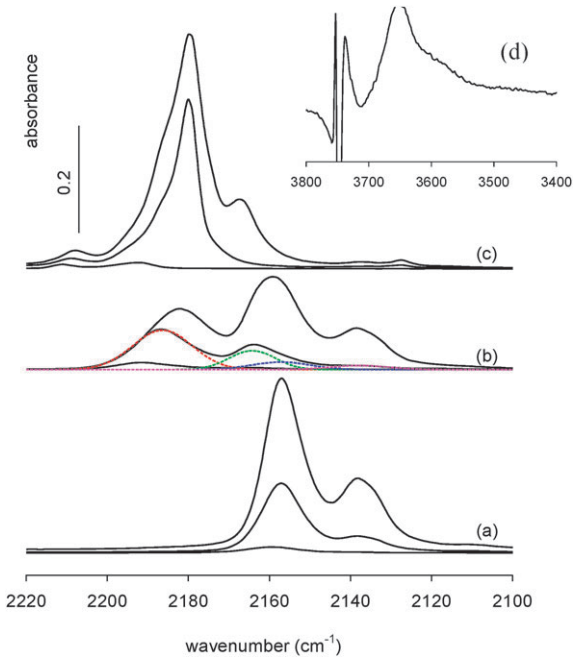

Fig. 9 Difference FTIR spectra (ν(CO) range) after addition of 25, 200 and 550 μmol g^{-1} of CO on (a) SBA-15; (b) Ti-SBA-4; (c) TiO_2; (d) ν(OH) range for Ti-SBA-4 after addition of 200 μmol g^{-1} CO.

dehydroxylation with the removal of the H-bonded silanols by condensation ($\equiv$Si–OH + $\equiv$Si–OH → $\equiv$Si–O–Si$\equiv$ + H_2O). Liu *et al.*[44] reported, for a Cabosil silica with almost the same surface silanol density (2.8 ± 0.3 OH per nm^2), the loss of about 1/3 of the silanols by dehydroxylation between 100 °C and 450 °C. We can therefore hypothesize a concentration of silanol, (after dehydration at 450 °C) of *ca.* 2 mmol g^{-1}. The maximum theoretical TiO_2 loading after the 1st grafting, assuming a monodentate grafting (one Ti on one Si–OH) should therefore be about 14 wt% which is very close to our experimental value (12 wt%). It indicates that all the Si–OH groups, whatever their location (in the micropores, in the mesopores or on the external surface) react during the grafting step.

During the pretreatment at 450 °C that preceded the 2nd grafting, some of the Si–OH are recovered due to the formation of TiO_2 domains upon calcination, but these domains are expected to be dehydroxylated. This is confirmed by the FTIR study which shows, in the ν(OH) region, no bands at 3720 and 3675 cm^{-1} characteristic of the stretching mode of O–H in TiO_2.[39,45] It means that the subsequent grafting can only occur on the TiO_2 free surface. This is probably the reason why the amount of grafted TiO_2 decreases with the number of graftings especially after the second grafting.

Nature and localization of the TiO_2 phase

Most of the experimental results are consistent and converge to indicate the formation of small (about 2 nm), mostly amorphous TiO_2 domains, whose size increases with the TiO_2 loading:

– the absence of crystalline TiO_2 particles larger than 2 nm (XRD),

– the presence of a few very small (*ca.* 2 nm) crystalline particles (high magnification TEM),

– a coordination of Ti that differs significantly from that of bulk TiO_2 with a majority of 5-fold coordinated Ti atoms (EXAFS and XANES),

– a slight increase in the coordination of Ti (EXAFS), and in the size of the TiO_2 domains (UV-vis spectroscopy), with the number of graftings.

However, some of the experimental results may seem contradictory. FTIR of adsorbed CO point out the presence of accessible silanol groups after 4 graftings, which means that the silica surface is only partially coated with TiO_2. Conversely, energy-filtered TEM tends to indicate an homogeneous coating (at the nm scale) of the silica surface. The most probable explanation comes from the 2D nature of the TEM images. In the TEM image of a SBA-15 material, each channel is actually the projection of several pores and, although in each pore the TiO_2 coating is discontinuous, the overlay of these discontinuous coatings may appear continuous on the 2D projection of the TEM images. To clarify this aspect, a sketch of the side, 3D and front view of a Ti-grafted SBA is shown on Fig. 10.

Several authors have proposed that the TiO_2 nanoparticles are located in the microporous corona of the SBA-15 material and that the small size of the corona cavities helps stabilize small, Si-doped, TiO_2 domains.[12,18] However, our results (energy-filtered TEM and N_2-sorption) tend to indicate that these particles are mainly located on the surface (or close to the surface) of the mesopores and that they are accessible to probe molecules (FTIR of adsorbed CO). This is not really surprising if one considers that, during the grafting step, most of the silanol groups (independently of their localization) react with titanium alkoxide to form $\equiv$Si–OTi$(OR)_3$. As the mesoporous surface area is significantly higher than the microporous surface area (by a factor of 3 or higher, see Table 1), Ti atoms are expected to be mostly located in the mesopores after the grafting step and a migration in the micropores during calcination is unlikely. An homogeneous distribution of the TiO_2 domains all over the surface is also consistent with the fact that the decrease in the surface area with the number of grafting is only a few percents higher for the microporous than for the mesoporous surface area (see Table 1).

The discrepancy between the results reported here and in the papers of Wang *et al.*[12] and Perathoner *et al.*[18] may be due to the dehydration temperature used prior to grafting. Indeed, in the present work we chose a high dehydration temperature (450 °C) to ensure the complete removal of adsorbed water from the surface and more specifically from the micropores.[21]

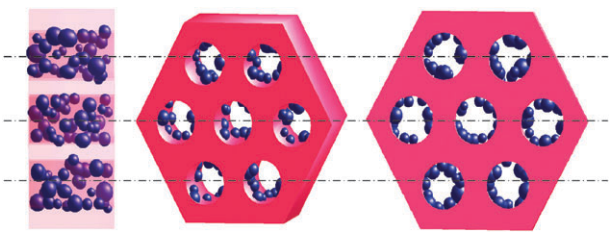

Fig. 10 Sketch showing the side- (a), 3D- (b) and front- (c) views of a SBA-15 material (light gray) coated with TiO_2 particles (dark gray).

The significantly lower dehydration temperatures used by Perathoner *et al.* and Wang *et al.* (80 °C and 140 °C in ref. 18 and 300 °C in ref. 12) could be insufficient to remove all the physisorbed water from the micropores and, as a consequence, would promote the formation of the titania nanoparticles in the micropores.

Conclusion

TiO_2/SBA-15 materials were prepared by successive graftings (1 to 4) of titanium isopropoxide on dehydrated SBA-15. Characterization of the obtained materials by XANES and EXAFS indicates that the grafted titanium atoms are mainly located in TiO_2 nanodomains. Characterization by TEM and XRD shows that these TiO_2 domains are mostly amorphous (crystallization to anatase is observed only after calcination at 900 °C). Moreover, the characterization by FTIR of adsorbed CO of the sample obtained after 4 graftings reveals the presence of surface sites characteristic of silica, titania and possibly of a mixed silica–titania phase. This result indicates that, even after 4 graftings, the silica surface is only partially coated by titania. The regular decrease in the pore diameter with the number of graftings together with the Energy-Filtered TEM characterization of the sample obtained after 4 graftings indicate that the TiO_2 nanodomains are mostly located on (or close to) the mesopore surface. We propose that the localization in the mesopores (rather than in the microporous corona as previously reported in ref. 12, 18) is due to the fact that, prior to each grafting, the (TiO_2)/SBA-15 sample was dehydrated at high temperature (450 °C) to ensure the complete removal of physisorbed water from the micropores. This localization is an advantage for applications as a catalyst support, as it improves the accessibility to the TiO_2 domains. Moreover, the dehydration at high temperature changes the localization of the TiO_2 particles but preserves the high dispersion of the TiO_2 phase (since the size of the TiO_2 nanodomains is 2 nm or less in this work and in ref. 18).

Acknowledgements

This work was supported by the ANR program JCJC (ANR-05-JCJC-0216-01) and the Japanese–French GDRI ECSAW CNRS & AIST). Vincent Richard is gratefully acknowledged for the TEM images. XAS experiments were performed under the approval of the Photon Factory Advisory Committee (proposal no. B2007G162).

Notes and references

1 G. Qi and R. T. Yang, *Appl. Catal., B*, 2003, **44**, 217–225.
2 J. A. Wang, A. Cuan, J. Salmones, N. Nava, S. Castillo, M. Morán-Pineda and F. Rojas, *Appl. Surf. Sci.*, 2004, **230**, 94–105.
3 M. Haruta, *Catal. Today*, 1997, **36**, 153–166.
4 J. Ramirez, G. Macias, L. Cedeno, A. Gutierrez-Alejandre, R. Cuevas and P. Castillo, *Catal. Today*, 2004, **98**, 19–30.
5 M. Breysse, C. Geantet, P. Afanasiev, J. Blanchard and M. Vrinat, *Catal. Today*, 2008, **130**, 3–13.
6 Y. Chen, Y. Huang, J. Xiu, X. Han and X. Bao, *Appl. Catal., A*, 2004, **273**, 185–191.
7 W. Wang and M. Song, *Microporous Mesoporous Mater.*, 2006, **96**, 255–261.
8 A. M. Busuioc, V. Meynen, E. Beyers, M. Mertens, P. Cool, N. Bilba and E. F. Vansant, *Appl. Catal., A*, 2006, **312**, 153–164.
9 M. V. Landau, L. Vradman, X. Wang and L. Titelman, *Microporous Mesoporous Mater.*, 2005, **78**, 117–129.
10 W. Yan, S. M. Mahurin, B. Chen, S. H. Overbury and S. Dai, *J. Phys. Chem. B*, 2005, **109**, 15489–15496.
11 V. Schwartz, D. R. Mullins, W. Yan, H. Zhu, S. Dai and S. H. Overbury, *J. Phys. Chem. C*, 2007, **111**, 17322–17332.
12 W. Wang and M. Song, *J. Non-Cryst. Solids*, 2006, **352**, 3153–3157.
13 E. Santacesaria, M. Cozzolino, M. Di Serio, A. M. Venezia and R. Tesser, *Appl. Catal., A*, 2004, **270**, 177–192.
14 Z. Luan and L. Kevan, *Microporous Mesoporous Mater.*, 2001, **44–45**, 337–344.
15 D. Sun, Z. Liu, J. He, B. Han, J. Zhang and Y. Huang, *Microporous Mesoporous Mater.*, 2005, **80**, 165–171.
16 A. Galarneau, N. Cambon, F. Di Renzo, R. Ryoo, M. Choi and F. Fajula, *New J. Chem.*, 2003, **27**, 73–79.
17 R. Zukerman, L. Vradman, L. Titelman, C. Weidenthaler, M. V. Landau and M. Herskowitz, *Microporous Mesoporous Mater.*, 2008, **116**, 237–245.
18 S. Perathoner, P. Lanzafame, R. Passalacqua, G. Centi, R. Schlögl and D. S. Su, *Microporous Mesoporous Mater.*, 2006, **90**, 347–361.
19 D. Zhao, Q. Huo, J. Feng, B. F. Chmelka and G. D. Stucky, *J. Am. Chem. Soc.*, 1998, **120**, 6025–6036.
20 M. Baca, E. de la Rochefoucauld, E. Ambroise, J.-M. Krafft, R. Hajjar, P. P. Man, X. Carrier and J. Blanchard, *Microporous Mesoporous Mater.*, 2008, **110**, 232–241.
21 E. F. Vansant, P. Van Der Voort and K. C. Vrancken, *Characterization and Chemical Modification of the Silica Surface*, Elsevier, Amsterdam, 1995.
22 T. Ohno, K. Sarukawa, K. Tokieda and M. Matsumura, *J. Catal.*, 2001, **203**, 82–86.
23 S. Biswas, M. F. Hossain, T. Takahashi, Y. Kubota and A. Fujishima, *Phys. Status Solidi A*, 2008, **205**, 2023–2027.
24 J. I. Pankove, *Optical Processes in Semiconductors*, Dover Publications Inc, New York, 1970.
25 M. Newville, *J. Synchrotron Radiat.*, 2001, **8**, 322–324.
26 B. Ravel and M. Newville, *J. Synchrotron Radiat.*, 2005, **12**, 537–541.
27 B. Ravel, *J. Synchrotron Radiat.*, 2001, **8**, 314–316.
28 J. J. Rehr and R. C. Albers, *Rev. Mod. Phys.*, 2000, **72**, 621–654.
29 N. N. Trukhan, A. A. Panchenko, E. Roduner, M. S. Mel'gunov, O. A. Kholdeeva, J. Mrowiec-Bialon and A. B. Jarzebski, *Langmuir*, 2005, **21**, 10545–10554.
30 M. Kruk, M. Jaroniec, C. H. Ko and R. Ryoo, *Chem. Mater.*, 2000, **12**, 1961–1968.
31 F. Schüth, A. Wingen and J. Sauer, *Microporous Mesoporous Mater.*, 2001, **44–45**, 465–476.
32 S. Monticone, R. Tufeu, A. V. Kanaev, E. Scolan and C. Sanchez, *Appl. Surf. Sci.*, 2000, **162–163**, 565–570.
33 G. Lassaletta, A. Fernandez, J. P. Espinos and A. R. Gonzalez-Elipe, *J. Phys. Chem.*, 1995, **99**, 1484–1490.
34 X. Gao and I. E. Wachs, *Catal. Today*, 1999, **51**, 233–254.
35 X. Gao, S. R. Bare, J. L. G. Fierro, M. A. Banares and I. E. Wachs, *J. Phys. Chem. B*, 1998, **102**, 5653–5666.
36 Z. Y. Wu, G. Ouvrard, P. Gressier and C. R. Natoli, *Phys. Rev. B: Condens. Matter*, 1997, **55**, 10382–10391.
37 F. Farges, G. E. Brown Jr. and J. J. Rehr, *Phys. Rev. B: Condens. Matter*, 1997, **56**, 1809–1819.
38 A. Zecchina, C. Lamberti and S. Bordiga, *Catal. Today*, 1998, **41**, 169–177.
39 K. Hadjiivanov, J. Lamotte and J. C. Lavalley, *Langmuir*, 1997, **13**, 3374–3381.
40 B. Bonelli, M. Cozzolino, R. Tesser, M. Di Serio, M. Piumetti, E. Garrone and E. Santacesaria, *J. Catal.*, 2007, **246**, 293–300.
41 L. Shi, Y. Zou and H. He, *Chem. Lett.*, 2001, 1164–1165.
42 K. Zhu, Z. Ma, Y. Zou, W. Zhou, T. Chen and H. He, *Chem. Commun.*, 2001, 2552–2553.
43 R. Mueller, H. K. Kammler, K. Wegner and S. E. Pratsinis, *Langmuir*, 2003, **19**, 160–165.
44 C. C. Liu and G. E. Maciel, *J. Am. Chem. Soc.*, 1996, **118**, 5103–5119.
45 K. Hadjiivanov, B. M. Reddy and H. Knözinger, *Appl. Catal., A*, 1999, **188**, 355–360.

